Journal of Molecular Catalysis A: Chemical 314 (2009) 88–94

Journal of Molecular Catalysis A: Chemical

journal homepage: www.elsevier.com/locate/molcata

Kinetic modeling based on the non-linear regression analysis for the degradation of Alizarin Red S by advanced photo Fenton process using zero valent metallic iron as the catalyst

L. Gomathi Devi*, K.E. Rajashekhar, K.S. Anantha Raju, S. Girish Kumar

Department of Post Graduate Studies in Chemistry, Central College Campus, Dr. B.R. Ambedkar Veedi, Bangalore University, Bangalore 560001, India

ARTICLE INFO

Article history:
Received 3 July 2009
Received in revised form 21 August 2009
Accepted 24 August 2009
Available online 31 August 2009

Keywords:
Advanced photo Fenton process
Zero valent metallic iron
Alizarin Red S
Ammonium persulfate
Kinetic/mathematical modeling

ABSTRACT

The degradation of Alizarin Red S (ARS), an anthraquinone dye was investigated by advanced photo Fenton process using zero valent metallic iron (ZVMI) powder as the catalyst with symmetrical peroxides like hydrogen peroxide (HP)/ammonium persulfate (APS) as the oxidants. APS is proved to be a better oxidant compared to HP as it provides efficient acidic medium which is critical for Fenton process. A kinetic/mathematical model was developed based on the non-linear regression analysis and the validity of the model was tested by comparing the observed experimental values with the theoretically calculated data. The rate equation obtained was found to be a function of iron dosage, oxidant and dye concentration at pH 3.

$$k = 0.2456[\mathrm{Fe}]^{0.21}[\mathrm{APS}]^{0.15}[\mathrm{ARS}]^{-0.76}$$

$$k = 0.58[\mathrm{Fe}]^{0.12}[\mathrm{HP}]^{0.10}[\mathrm{ARS}]^{-0.86}$$

The degradation pathway was followed by UV–vis spectroscopy and GC–MS techniques. Based on the intermediates analyzed, a probable degradation mechanism has been proposed.

1. Introduction

In the textile industry, it is estimated that 10–15% of the dye is lost during the dyeing and finishing operations and is released as textile effluents. Dyes in wastewater can also cause eutrophication and carcinogenic byproducts that are formed through oxidation, hydrolysis or by other chemical reactions. Traditional methods in treating the wastewater include flocculation, carbon adsorption, reverse osmosis and activated sludge processes. These methods have difficulties in the complete destruction of the pollutants and they simply transfer the pollutants from one phase to another. Advanced oxidation process (AOP) based on the in situ generation of hydroxyl radicals is a promising technique for the treatment of wastewater containing dyes. The common AOPs used are (1) semiconductor photocatalysis: TiO_2 or ZnO/UV [1–6] and (2) Fenton and photo Fenton-like processes: Fe^{2+} or Fe^{3+}/H_2O_2 or APS/UV [7–11]. Photo Fenton processes have gained the large scope due to its cost effective, easy availability of reagents and the process can be efficiently carried out at laboratory conditions. However the removal of iron ions at the end of wastewater treatment is costly and requires man power. Lucking et al. [12] tested iron powder, graphite and activated carbon for the catalytic process for the oxidation of 4-chloropenol in the solution with H_2O_2. They concluded that iron powder could be used to replace iron salts as a catalyst in photo Fenton process. From the environmental point of view, the advantage of using metallic iron powder (Fe^0) instead of iron salts is that, the concentration of iron ions in the wastewater after the treatment can be significantly reduced. Moreover, use of Fe^0 as catalyst instead of iron salts prevents the additional anion loading in the treatment of wastewater. The residual iron powder can be easily removed after the treatment and can be easily recycled. The degradation of ARS using different photocatalysts under different experimental conditions is reported by several research groups [13–29]. The present research work focuses on the degradation of synthetic dye ARS using zero valent metallic iron (ZVMI) of 300-mesh size as a source to generate Fe^{2+} ions. A kinetic/mathematical model was developed based on the non-linear regression analysis and the validity of the model was tested by comparing the experimental and theoretically calculated data. Although this kind of model was applied for TiO_2 photocatalysis by few research groups [30–34], so far it is least attempted for photo Fenton process.

* Corresponding author. Tel.: +91 080 22961336; fax: +91 080 22961331.
E-mail address: gomatidevi_naik@yahoo.co.in (L.G. Devi).

1381-1169/$ – see front matter © 2009 Elsevier B.V. All rights reserved.
doi:10.1016/j.molcata.2009.08.021

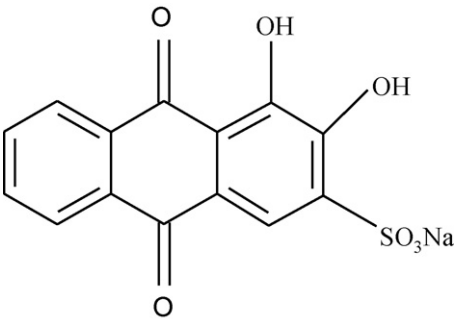

Fig. 1. Structure of ARS.

2. Materials and methods

2.1. Materials

ARS, ZVMI (95% purity, 300-mesh size, electrolytic), APS and HP (50%, w/v) were supplied from S D Fine Chemicals, Bombay, India and were used as received. The molecular formula of ARS is $C_{14}H_7NaO_7S{\cdot}H_2O$ (C.I. 58005) and molecular weight is 360.28 and has λ_{max} at 514–520 nm. The structure of the dye is shown in Fig. 1.

2.2. Irradiation procedure

Advanced photo Fenton process (APFP) was carried out at room temperature using a circular glass reactor whose surface area is 176.6 cm^2. The reactor was placed in a thermostat at a temperature of at 298 ± 5 K. Artificial light source used in the present study is 125 W medium pressure mercury vapor lamp. The photon flux of the light source is 7.75 mW/cm^2 as determined by ferrioxalate actinometry, the wavelength of which peaks around 350–400 nm. In a typical experiment, 200 mg/L of the ARS dye solution is taken in the reactor and desired amount of iron powder (50 mg/L) and oxidants (APS = 200 mg/L or HP = 100 mg/L) are added before the beginning of the experiment. The lamp was warmed for 10 min to reach constant output. The irradiation was carried out by direct focusing the light into the reaction mixture in open air condition at a distance of 29 cm. All the experiments were performed using double distilled water. pH of the solution was adjusted either by adding dilute NaOH or H_2SO_4 and measured using Systronics digital pH meter.

2.3. Analytical methods

The solution of 5 ml is taken out from the reactor at definite time intervals and centrifuged. The centrifugates were analyzed by UV–vis spectroscopic technique using Shimadzu UV-1700 Pharmaspec UV–vis spectrophotometer. The centrifugate was extracted into non-aqueous ether medium and 1 μL was subjected to GC–MS analysis (using GC-MS-QP-5000 Shimadzu) and Thermo Electron Trace GC ultra coupled to a DSQ mass spectrometer equipped with an Alltech ECONO-CAP-EC-5 capillary column (30 m × 0.25 mm i.d. × 0.25 mm film thickness) was used. Pure helium was used as the carrier gas at a flow rate of 1.2 ml/min. The injector/transfer line/trap temperature was 220/250/200 °C respectively. Electron impact ionization was carried out at 70 eV.

2.4. Estimation of iron ions in the solution

The concentration of Fe^{2+} ions leached into the bulk of the solution by the iron surface was quantitatively analyzed by a colorimetric method using o-phenanthroline as a colorimetric reagent using acetic acid and sodium acetate buffer. Hydroquinone was added so as to reduce the available Fe^{3+} to Fe^{2+} ions in the solution. The absorbance of Fe (II)–phenanthroline complex was measured at 510 nm. The concentration of photo-generated Fe^{2+} ions after the degradation process was estimated by the standard calibration curve.

3. Results and discussion

Heterogeneous photo Fenton process shows enhanced activity compared to their homogeneous counterparts, probably due to the faster reduction of Fe^{3+} ions to Fe^{2+} ions on the iron surface [35,36]:

$$2Fe^{3+} + Fe^0 \rightarrow 3Fe^{2+} \quad (1)$$

The various reactions taking place between $Fe^0/Fe^{2+}/Fe^{3+}$ with the HP and APS are illustrated as follows:

Iron powder undergoes oxidation in acidic pH to give ferrous ion (Fe^{2+}):

$$Fe^0 \xrightarrow{H^+} Fe^{2+} \quad (2)$$

Iron powder reacts with HP to give Fe^{2+} ions which are partially adsorbed on iron surface, which on reaction with HP generates hydroxyl radicals.

$$Fe^0 + H_2O_2 \rightarrow Fe^{2+}\text{-surface} \quad (3)$$

$$Fe^{2+}\text{-surface} + H_2O_2 \rightarrow Fe^{3+} + HO^{\bullet} + HO^- \quad (4)$$

Iron powder reacts with oxidants, generating Fe^{2+} ions which diffuse into the bulk of the solution.

$$Fe^0 + H_2O_2 \rightarrow Fe^{2+} + 2HO^- \quad (5)$$

$$Fe^0 + S_2O_8^{2-} \rightarrow Fe^{2+} + 2SO_4^{2-} \quad (6)$$

The Fe^{2+} so produced reacts with oxidants to generate free radicals. During this process Fe^{2+} is oxidized to Fe^{3+}.

$$Fe^{2+} + H_2O_2 \rightarrow Fe^{3+} + OH^{\bullet} + OH^- \quad (7)$$

$$Fe^{2+} + S_2O_8^{2-} \rightarrow Fe^{3+} + SO_4^{2-} + SO_4^{-\bullet} \quad (8)$$

Ferric ions (Fe^{3+}) so formed can either react with water or with H_2O_2 in the following way:

(i) Fe^{3+} ions react with water to form hydroxo complex, which on UV-irradiation generates Fe^{2+} and hydroxyl radicals.

$$Fe^{3+} + H_2O \Leftrightarrow [Fe(OH)^{2+}] + H^+ \quad (9)$$

$$[Fe(OH)^{2+}] + h\nu \rightarrow Fe^{2+} + HO^{\bullet} \quad (10)$$

(ii) Fe^{3+} reacts with H_2O_2 to generate Fe^{2+} and hydro peroxyl radicals. The radical so formed has the ability to reduce Fe^{3+} ions to Fe^{2+}.

$$Fe^{3+} + H_2O_2 \rightarrow Fe^{2+} + H^+ + HO_2^{\bullet} \quad (11)$$

$$Fe^{3+} + HO_2^{\bullet} \rightarrow Fe^{2+} + O_2 + H^+ \quad (12)$$

Fe^{3+} reacts with persulfate anion, two molecules of sulfate radicals are produced which react with water to generate hydroxyl radicals.

$$Fe^{3+} + S_2O_8^{2-} \rightarrow Fe^{2+} + 2SO_4^{-\bullet} \quad (13)$$

$$SO_4^{-\bullet} + H_2O \rightarrow SO_4^{2-} + OH^{\bullet} + H^+ \quad (14)$$

3.1. Effect of pH

Kang et al. [37] reported that the pollutants can be decolorized efficiently in photo Fenton process only under acidic conditions. The experiments were performed in the pH range of 0.5–9.5. The rate constant (calculated from the plot of $-\log C/C_0$ versus time) for

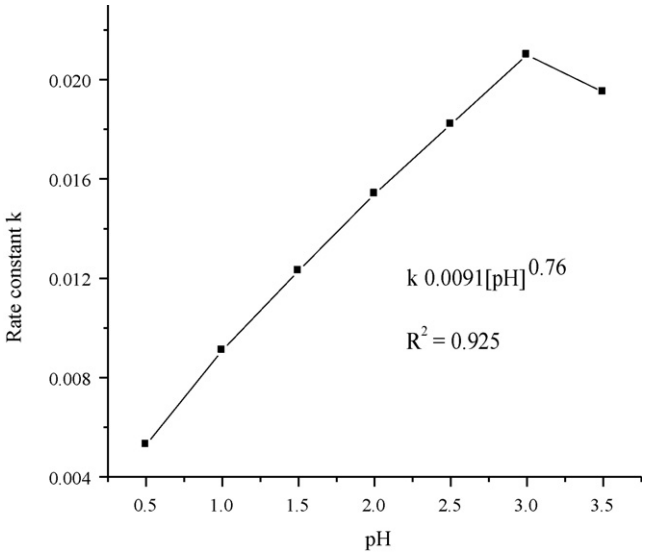

Fig. 2. Plot of rate constant versus pH for the degradation of ARS (Fe^0 = 50 mg/L, APS = 200 mg/L and ARS = 200 mg/L).

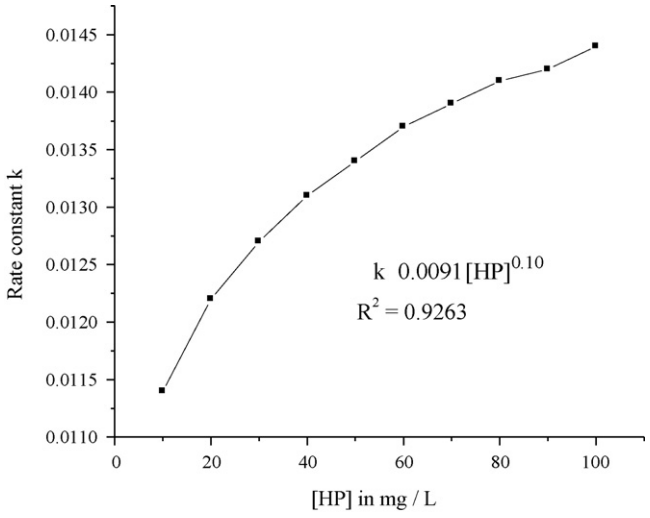

Fig. 3. Plot of rate constant versus concentration of HP (Fe^0 = 50 mg/L, ARS = 200 mg/L and pH 3).

the degradation at pH 3 is found to be 0.021 min^{-1} for Fe^0/APS/UV as shown in Fig. 2. At pH 3, the concentration of Fe^{3+} ions and $Fe[OH]^{2+}$ complexes is the dominating photoactive species in almost equal proportions. The decrease in this optimum pH leads to decrease in the concentration of $Fe[OH]^{2+}$ complexes and it can also result in the precipitation of ferrous ion as oxy hydroxides.

The various photoactive species of iron formed at different conditions of pH are $Fe[H_2O]_6^{3+}$ (pH 1–2), $Fe[OH][H_2O]_5^{2+}$ (pH 2–3) and $Fe[OH]_2[H_2O]_4^{+}$ (pH 3–4) [9]. The lower rate constant at pH 0.5 is mainly due to the excess H^+ ions in the solution acting as hydroxyl radical scavenger [38,39].

$$H^+ + OH^\bullet + e^- \rightarrow H_2O \quad (15)$$

The non-linear relation between the rate constant (k) for the degradation of the dye and pH can be modeled with simple empirical power-law type relationship as follows:

$$k\alpha[pH]^n$$

where n is an integer.

Fitting the experimental data with the above formulae we get

$$k\alpha[pH]^{0.76} \quad \text{or} \quad k = x[pH]^{0.76}$$

where x is a constant, which is arbitrarily chosen as 0.0091 to fit the experimental data.

$$k = 0.0091[pH]^{0.76}$$

At pH (≥7), dye shows resistance to degradation due to the coagulation of Fe^{3+} complex molecules formed in the reaction which inhibits the catalytic reaction of Fe^{2+} ions with the oxidants. Further at high pH, precipitation of iron oxy hydroxides takes place which gets deposited on the surface of iron powder preventing the process of electron transfer between the catalyst and the oxidant thereby reducing the generation of hydroxyl radicals in the solution. Therefore APFP experiments were optimized at pH 3.

3.2. Effect of oxidants

The present study investigates the application of HOOH (hydrogen peroxide) and $S_2O_8^{2-}$ (peroxy disulfate) which are symmetrical peroxides and can be potential oxidants in the light induced reaction processes. Persulfate can also generate free radicals like sulfate and hydroxyl radicals which provide free radical mechanism similar to hydroxyl radical pathways generated in the Fenton's chemistry. Sulfate radical is one of the strongest oxidizing species in aqueous media with a redox potential of 2.6 V which is next only to the hydroxyl free radical whose redox potential is 2.8 V. The sulfate radical anions produced in the case of APS show various possible reaction mechanisms in the process of mineralization. (i) Abstraction of hydrogen atom from the saturated carbon; (ii) capable of adding to the unsaturated compounds; (iii) it can remove an electron from the anions and neutral molecules [40,41]. These attributes combine to make persulfate a viable option for the chemical oxidation of a broad range of contaminants.

The influence of oxidants on the degradation was investigated by maintaining the other reaction parameters constant (Iron powder dosage = 50 mg/L, dye concentration = 200 mg/L at pH = 3.0). The concentration of H_2O_2 was varied from 50 to 200 mg/L and was optimized at 100 mg/L as shown in Fig. 3. The increase in the concentration of oxidizing agent enhances the generation of hydroxyl radicals and hence increase in the rate constant is observed.

The non-linear relation between the degradation of the dye and concentration of the oxidants using power-law empirical type relationship is given by

$$k\alpha[HP]^{0.10} \quad \text{or} \quad k = 0.0091[HP]^{0.10}$$

Similarly, a series of experiments in the range 25–300 mg/L were carried using APS and were optimized at 200 mg/L (Fig. 4).

$$k\alpha[APS]^{0.15} \quad \text{or} \quad k = 0.0091[APS]^{0.15}$$

Beyond the optimum concentration the rate constant decreases for both the oxidants. This can be due to the recombination of excess hydroxyl radicals generated or the radicals might get involved in the unwanted reaction pathways.

The rate constant calculated for the process Fe^0/APS/UV is ~1.5 times higher than Fe^0/H_2O_2/UV process. This is mainly attributed to the influence of oxidants on the final pH of the reaction which is explained as follows: the final pH of the solution was 3.6 with H_2O_2 (100 mg/L) as an oxidant while final pH was reduced to 2.9 for APS (200 mg/L). The iron ions leached after the end of dye degradation process is 15.5 mM for Fe^0/H_2O_2/UV process which is higher compared to Fe^0/APS/UV (9.1 mM). Thus the excess iron ions might serve as hydroxyl radical scavenger. Since APS provides better acidic pH which is essential for Fenton process, it accelerates the rate of reaction compared to H_2O_2.

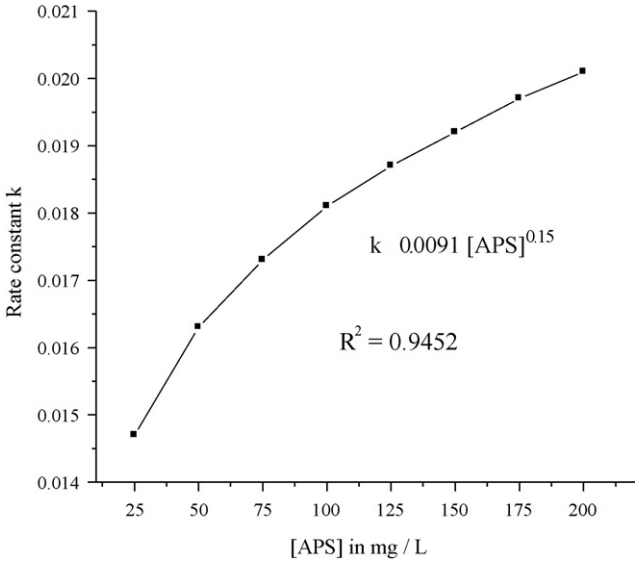

Fig. 4. Plot of rate constant versus concentration of APS (Fe^0 = 50 mg/L, ARS = 200 mg/L and pH 3).

3.3. Effect of catalyst loading

The degradation efficiency was found to be 15 and 26% respectively with H_2O_2/UV and APS/UV process for 2 h of irradiation. This is due to the direct photolysis of oxidants in the presence of UV light. However complete degradation with higher efficiency was achieved by the use of iron surface in the presence of oxidants in APFP. The iron surface catalytically decomposes the oxidants to respective free radicals/ions at a faster rate to generate more hydroxyl radicals under UV light. A series of experiments were performed in the range 10–100 mg/L and was optimized at 50 mg/L for both the oxidants as shown in Figs. 5 and 6.

The non-linear relation between the degradation of the dye and catalyst dosage using power-law empirical type relationship is given by

$k\alpha[\mathrm{Fe}]^{0.21}$ or $k = 0.0091[\mathrm{Fe}]^{0.21}$ for APS as oxidant.

$k\alpha[\mathrm{Fe}]^{0.12}$ or $k = 0.0091[\mathrm{Fe}]^{0.12}$ for HP as oxidant.

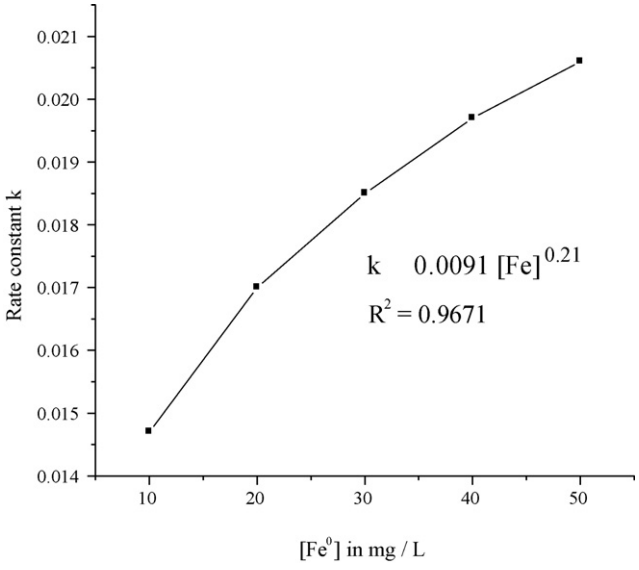

Fig. 5. Plot of rate constant versus iron dosage using APS as oxidant (APS = 200 mg/L, ARS = 200 mg/L and pH 3).

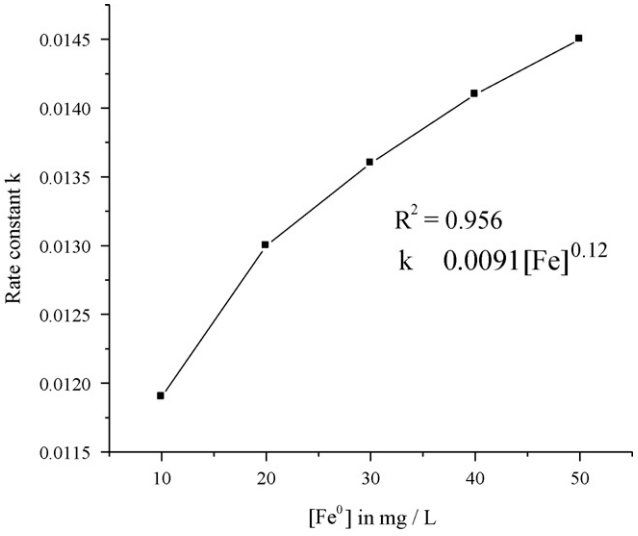

Fig. 6. Plot of rate constant versus iron dosage using HP as oxidant (HP = 100 mg/L, ARS = 200 mg/L and pH 3).

In contrast, overloading of the catalyst hinders the degradation efficiency. This is due to: (i) higher concentration of the catalyst results in turbidity which hinders the UV light penetration [42]. (ii) High dosage of iron powder increases the concentration of Fe^{2+} ions in the solution which can also act as hydroxyl radical scavenger.

$$Fe^{2+} + OH^{\bullet} \rightarrow Fe^{3+} + OH^{-} \quad (16)$$

Increase in the dosage of iron powder shifts the reaction medium from acidic to alkaline medium which affects the degradation rate. The shift in the pH depends mainly on the nature of the oxidants which can be explained as follows: when the catalyst loading was varied from 50 to 200 mg, the final pH of the reaction mixture is 3.6 and when it is increased to 400 mg, pH of the solution changes to 4.8 with HP as oxidant. At this condition, turbidity in the reaction mixture is observed. With further increase in the catalyst loading 600 mg, excess iron precipitates as iron oxy hydroxides and the precipitate separates from the true solution and the pH of the solution changes to 5.6. The final pH of the reaction medium was 3.9 for higher concentration of iron powder with APS as an oxidant. Hence it can be concluded that APS effectively inhibited the precipitation of iron powder providing excess acidity to the reaction medium.

3.4. Effect of initial dye concentration

In the photo Fenton process, change in the dye concentration affects the degradation process significantly. Therefore experiments were performed at different initial dye concentrations by maintaining the other reaction parameters constant as shown in Figs. 7 and 8. Beyond the optimum concentration (200 mg/L), the degradation efficiency decreases to 55% for higher initial dye concentration (500 ppm). This may be due to the fact that, as the dye concentration is increased, the number of hydroxyl radicals is not increased proportionally. Further high dye concentration prevents the UV light penetration into the depth of the solution there by decreasing the generation of hydroxyl radicals [43,44]. At high concentrations of dye, the active centers on the iron surface will be occupied by the dye molecules which are capable of reducing the catalyst surface itself by hindering the process of hydroxyl radical generation. Fe^0/APS/UV process showed better efficiency for the degradation of dye at higher concentration compared to Fe^0/H_2O_2/UV.

The non-linear relation between the dye degradation and dye concentration using power-law empirical type relationship is given

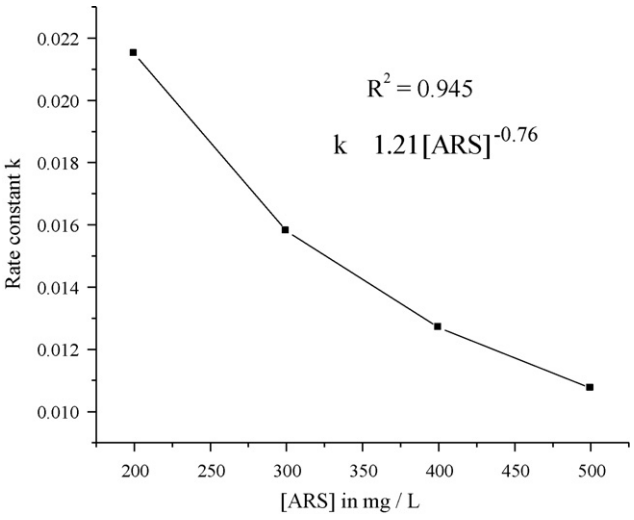

Fig. 7. Plot of rate constant versus ARS concentration using APS as oxidant (Fe^0 = 50 mg/L, APS = 200 mg/L and pH 3).

by

$k\alpha[\mathrm{ARS}]^{-0.76}$ or $k = 1.21[\mathrm{ARS}]^{-0.76}$ for APS as oxidant

$k\alpha[\mathrm{ARS}]^{-0.86}$ or $k = 1.38[\mathrm{ARS}]^{-0.86}$ for HP as oxidant

3.5. Development of rate equation

The photocatalytic degradation of ARS is assumed to be pseudo-first order reaction with respect to ARS concentration which is expressed as follows:

$$\frac{-d[\mathrm{ARS}]}{dt} = k_{\mathrm{APFP}}[\mathrm{ARS}] \quad (17)$$

where k_{APFP} is the rate constant for APFP.

The rate constant critically depends on iron dosage, oxidant concentration and initial concentration of the dye.

$$k = y[\mathrm{Fe}]^a[\mathrm{APS}]^b[\mathrm{ARS}]^c \quad (18)$$

with non-linear regression analysis the values of a, b and c are calculated and they are 0.21, 0.15 and −0.76 as discussed in the previous section. The value of 'y' is therefore found to be 0.2456. Substituting in Eq. (17):

$$k = 0.2456[\mathrm{Fe}]^{0.21}[\mathrm{APS}]^{0.15}[\mathrm{ARS}]^{-0.76} \quad (19)$$

Similarly for H_2O_2 as oxidant:

$$k = 0.58[\mathrm{Fe}]^{0.12}[\mathrm{HP}]^{0.10}[\mathrm{ARS}]^{-0.86} \quad (20)$$

The plots of experimentally observed and theoretically calculated rate constant values are shown in Figs. 9 and 10 for the degradation of ARS using APS and HP. The results from the plot reveal that the proposed kinetic model is well in agreement with the experimental ones.

The rate law by this kinetic modeling is theoretically predicted and varies with experimental conditions. But still this model provides the information about the effect of exact operational parameters.

3.6. Recycling efficiency of iron powder

The efficiency of iron powder was tested by recycling it for the degradation of ARS with respect to the optimized conditions as previously reported. After each run, fresh dye solution along with the

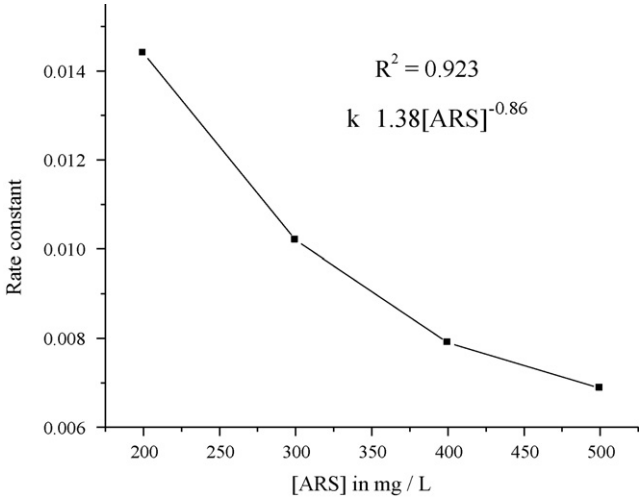

Fig. 8. Plot of rate constant versus ARS concentration using HP as oxidant (Fe^0 = 50 mg/L, HP = 100 mg/L and pH 3).

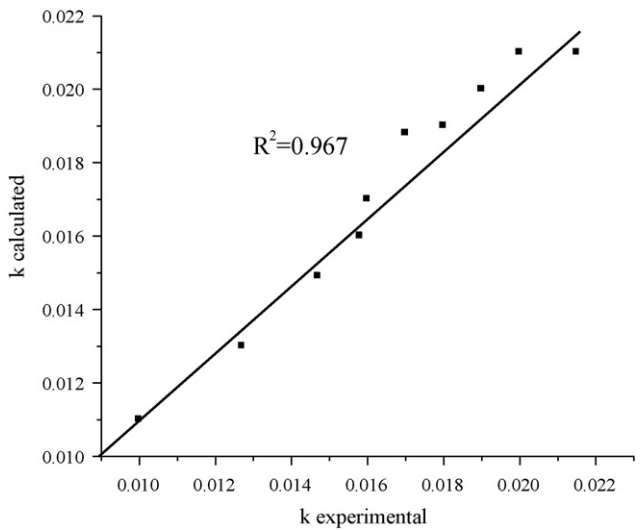

Fig. 9. Plot of calculated rate constant versus experimental rate constant for Fe^0/APS/UV process.

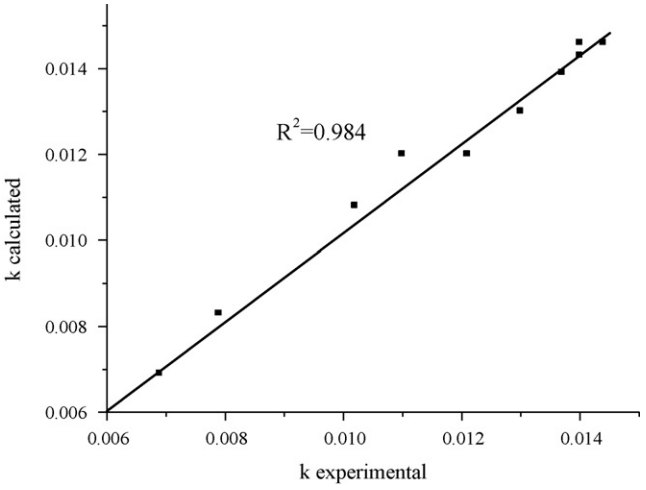

Fig. 10. Plot of calculated rate constant versus experimental rate constant for Fe^0/HP/UV process.

oxidant is replaced in the reactor using the same iron powder. It can be seen that iron powder retains its efficiency for the first five consecutive runs for both the oxidants (Fig. 11). After the fifth run, significant decrease in its efficiency was observed with APS compared to HP. This is because iron powder under acidic condition undergoes dissolution to give Fe^{2+} ions. The additional acidity provided by the APS increases the concentration of Fe^{2+} ions by the dissolution of iron powder. The oxidation of iron powder in the subsequent runs by APS might probably reduce the efficiency.

3.7. GC–MS analysis: degradation pathway for ARS

The hydroxyl radicals generated attacks at the site of reactive carbonyl group leading to the formation of pthalic acid (1), hydroxy benzene sulfonic acid (2) and dihydroxy benzene (3) which is confirmed by the presence of m/z peaks at 165, 174 and 110 respectively. This suggests that the degradation of ARS proceeds through the cleavage of anthraquinone moiety. The formation of pthalic acid during the degradation of ARS is in agreement with the previous reports [13–16]. After 75 min of UV irradiation, m/z peaks at 121, 94, 108 and 116 were attributed to the formation of

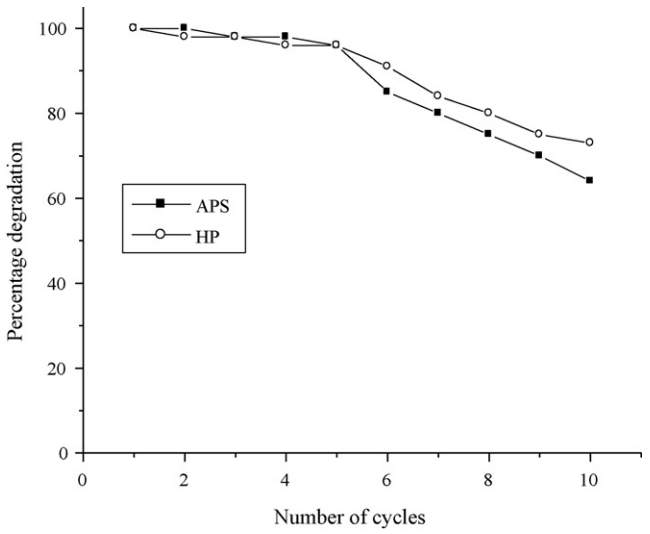

Fig. 11. Recycling efficiency of iron powder in the presence of different oxidants (Fe^0 = 50 mg/L, APS = 200 mg/L or HP = 100 mg/L, ARS = 200 mg/L at pH 3).

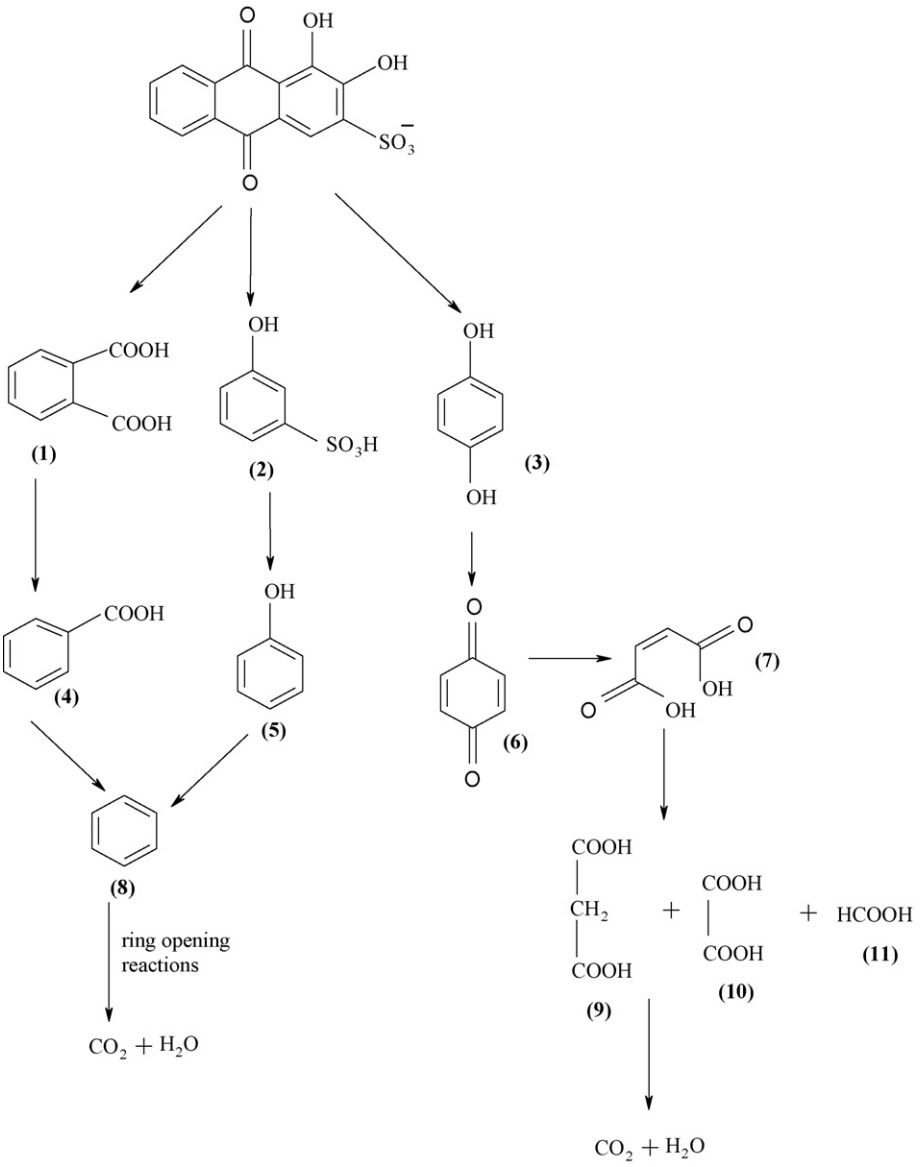

Scheme 1. Probable degradation pathway for ARS (Fe^0 = 50 mg/L, APS = 200 mg/L, ARS = 200 mg/L at pH 3).

benzoic acid (4), phenol (5), hydroquinone (6) and maleic acid (7). Few low intense peaks were left unaccounted. The decarboxylation and desulfonation of intermediate (1) and (2) might probably result in the formation of (4) and (5). The intermediate (3) might get oxidized to (6) and subsequent ring opening reaction can lead to the formation of (7) [35]. The intermediates (4) and (5) transform to benzene (8) which on subsequent reaction with hydroxyl radicals undergo complete degradation. The stepwise degradation of (7) leads to a series of aliphatic acids like malonic acid (9), oxalic acid (10) and formic acid (11) confirmed by the presence of peaks at 104, 90 and 46 respectively. Based on the intermediates obtained, probable degradation mechanism has been proposed (Scheme 1).

4. Conclusion

A kinetic modeling was developed based on the non-linear regression analysis for the degradation of ARS using advanced photo Fenton process driven by UV light. The influence of various reaction parameters like iron dosage, concentration of oxidants and dye is investigated in detail. APS proved to be better oxidant compared to HP as it provides a better acidic medium which is critical for Fenton process. The rate equation developed was found to be a function of iron dosage, oxidant and dye concentration at pH 3. The theoretically calculated rate constants were well in agreement with the experimentally obtained values justifying the significance of mathematical model. The photoproducts formed during the course of the reaction were analyzed by GC–MS technique and probable degradation mechanism has been proposed.

Acknowledgement

Financial assistance from UGC Major Research Project (2007–2010) is acknowledged.

References

[1] J. Yu, H. Yu, B. Cheng, C. Trapalis, J. Mol. Catal. A: Chem. 249 (2006) 135–142.
[2] J. Yu, L. Zhang, B. Cheng, Y. Su, J. Phys. Chem. C 111 (2007) 10582–10589.
[3] J. Yu, W. Liu, H. Yu, Cryst. Growth Des. 8 (2008) 930–934.
[4] J. Yu, Y. Su, B. Cheng, Adv. Funct. Mater. 17 (2007) 1984–1990.
[5] J. Yu, G. Wang, B. Cheng, M. Zhou, Appl. Catal. B: Environ. 69 (2007) 171–180.
[6] J. Yu, X. Yu, Environ. Sci. Technol. 42 (2008) 4902–4907.
[7] J.A.H. Melian, E.T. Rendon, J. Arana, J.M.D. Rodriguez, O.G. Diaz, J.P. Pena, Toxicol. Environ. Chem. 85 (2003) 61–73.
[8] N. Daneshvar, A.R. Khataee, J. Environ. Sci. Health Part A 41 (2006) 315–328.
[9] M. Neamtu, A. Yediler, I. Siminiceanu, A. Kettrup, J. Photochem. Photobiol. A: Chem. 161 (2003) 87–93.
[10] P. Papaolymerou, K. Ntampegliotis, A. Riga, V. Karayannis, V. Bontozoglou, J. Hazard. Mater. 136 (2006) 75–84.
[11] L.G. Devi, S.G. Kumar, K.M. Reddy, Cent. Eur. J. Chem. 7 (2009) 468–477.
[12] F. Lucking, H. Koser, M. Jank, A. Ritter, Water Res. 32 (1998) 2607–2614.
[13] P. Zucca, C. Vinci, F. Sollai, A. Rescigno, E. Sanjust, J. Mol. Catal. A: Chem. 288 (2008) 97–102.
[14] G. Liu, T. Wu, J. Zhao, Environ. Sci. Technol. 33 (1999) 2081–2087.
[15] G. Liu, X. Li, J. Zhao, H. Horikoshi, H. Hidaka, J. Mol. Catal. A: Chem. 153 (2000) 221–229.
[16] J. Gao, J. Yu, Q. Lu, X. He, W. Yang, Y. Li, L. Pu, Z. Yang, Dyes Pigments 76 (2008) 47–52.
[17] J. Ma, W. Song, C. Chen, W. Ma, J. Zhao, Y. Tang, Environ. Sci. Technol. 39 (2005) 5810–5815.
[18] B. Muktha, G. Madras, T.N.G. Row, U. Scherf, S. Patil, J. Phys. Chem. B 111 (2007) 7994–7998.
[19] C. Chen, X. Li, W. Ma, J. Zhao, H. Hidaka, N. Serpone, J. Phys. Chem. B 106 (2002) 318–324.
[20] D. Zhao, C. Chen, Y. Wang, H. Ji, W. Ma, L. Zang, J. Zhao, J. Phys. Chem. C 112 (2008) 5993–6001.
[21] T. Wu, G. Liu, J. Zhao, H. Hidaka, N. Serpone, J. Phys. Chem. B 103 (1999) 4862–4867.
[22] C. Chen, Q. Wang, P. Lei, W. Song, W. Ma, J. Zhao, Environ. Sci. Technol. 40 (2006) 3965–3970.
[23] Y. Yang, Q. Wu, Y. Guo, C. Hu, E. Wang, J. Mol. Catal. A: Chem. 225 (2005) 203–212.
[24] H. Lachheb, E. Puzenat, A. Houas, M. Ksibi, E. Elaloui, C. Guillard, J.M. Herrmann, Appl. Catal. B: Environ. 39 (2002) 75–90.
[25] A.M. Faouzi, B. Nasr, G. Abdellatif, Dyes Pigments 73 (2007) 86–89.
[26] H.S. Hilal, L.Z. Majjad, N. Zaatar, A.E. Hamouz, Solid State Sci. 9 (2007) 9–15.
[27] C. Guillard, H. Lachheb, A. Houas, M. Ksibi, E. Elaloui, J.M. Herrmann, J. Photochem. Photobiol. A: Chem. 158 (2003) 27–36.
[28] M. Panizza, G. Cerisola, Water Res. 43 (2009) 339–344.
[29] D. Zhao, C. Chen, Y. Wang, W. Ma, J. Zhao, T. Rajh, L. Zang, Environ. Sci. Technol. 42 (2008) 308–314.
[30] M.A. Behnajady, N. Modirshahla, Photochem. Photobiol. Sci. 5 (2005) 1078.
[31] M.A. Behnajady, N. Modirshahla, R. Hamzavi, J. Hazard. Mater. 133 (2006) 226–232.
[32] Y. Zang, R. Farnood, Appl. Catal. B: Environ. 57 (2005) 275–282.
[33] C. Galilndo, P. Jacques, A. Kalt, Chemosphere 45 (2001) 997–1005.
[34] T. Sauer, G.C. Neto, J.J. Jos'e, R.F.P.M. Moreira, J. Photochem. Photobiol. A. Chem. 249 (2002) 147–154.
[35] D.H. Bermer, A.E. Burgess, D. Houllmare, K.C. Namkung, Appl. Catal. B: Environ. 63 (2006) 15–19.
[36] L.G. Devi, K.S.A. Raju, S.G. Kumar, J. Environ. Monit. 11 (2009) 1397–1407.
[37] S.F. Kang, C.H. Liao, M.C. Chen, Chemosphere 46 (2002) 923–928.
[38] K. Barbusinski, J. Majewski, Polish J. Environ. Stud. 12 (2003) 151–155.
[39] L.G. Devi, S.G. Kumar, K.M. Reddy, C. Munikrishnappa, Desalination Water Treat. 4 (2009) 294–305.
[40] E. Evgenidou, I. Konstantinou, K. Fytianos, I. Poulios, Water. Res. 41 (2007) 2015–2027.
[41] P. Neta, V. Madhavan, H. Zemel, R.W. Fessemdem, J. Am. Chem. Soc. 99 (1977) 163–164.
[42] O.S.N. Sum, J. Feng, X. Hu, P.L. Yue, Top. Catal. 33 (2005) 233–242.
[43] L.G. Devi, S.G. Kumar, K.M. Reddy, C. Munikrishnappa, J. Hazard. Mater. 164 (2009) 459–467.
[44] K. Dutta, S. Mukhopadhyay, S. Bhattacharjee, B. Chaudhuri, J. Hazard. Mater. 84 (2001) 57–71.